Nanoscale

ROYAL SOCIETY OF CHEMISTRY

PAPER

View Article Online
View Journal

Check for updates

Cite this: DOI: 10.1039/d5nr05114b

Effect of biphilic pattern type, size and wettability ratio on atmospheric water collection

Konstantinos Taliantzis and Kosmas Ellinas *

Water scarcity is intensifying worldwide, driving the development of sustainable atmospheric water-harvesting strategies. Nature-inspired biphilic surfaces, integrating hydrophilic and hydrophobic areas, provide a promising solution by promoting controlled condensation and directional droplet transport. Although several biphilic pattern types have been proposed in the literature, there is no systematic study evaluating a series of different patterns in order to extract specific design guidelines for the biphilic patterning. In this work, we fabricate and evaluate surfaces with a series of different biphilic patterns, which exhibit different ratio of superhydrophobic/superhydrophilic area coverage and different working principle for drop capturing and collection in fog collection and drop nucleation and collection in dew collection. Biphilic patterning is realized on pre-designed, deterministic, micro-topographies (pillars, trapezoids, and honeycombs) which are fabricated using PDMS soft lithography. In fog collection, water collection rate (WCR) of superhydrophobic surfaces with pillars and trapezoids is improved compared to untreated PDMS, whereas after biphilic patterning, the WCR is not affected, emphasizing the importance of drop mobility in fog collection. In dew collection, performance is strongly dependent on the environmental conditions. At moderate conditions (relative humidity: 70% and temperature difference between the sample and the environment ΔT = 15 °C), biphilic surfaces with parallel stripes (width: 1000 μm, spacing: 2000 μm), which act as "water guides" driven by gravity and low surface coverage (35%), exhibit increased WCR by 156% compared to flat PDMS. From the fabrication point of view, the method presented here is PFAS-free and scalable, providing another pathway for the realization of water collection interfaces.

Received 4th December 2025,
Accepted 24th April 2026

DOI: 10.1039/d5nr05114b

rsc.li/nanoscale

Laboratory of Advanced Functional Materials and Nanotechnology, Department of Food Science and Nutrition, School of the Environment, University of the Aegean, Leoforos Dimokratias 66, Myrina 81400, Lemnos, Greece.
E-mail: kellinas@aegean.gr

Kosmas Ellinas

Dr Kosmas Ellinas, is Assistant Professor of Applied Physics and Nanotechnology at the DFNS, University of the Aegean. He has participated in more than 15 research projects (National, European, and private funding), several as PI or co-PI. He is the author or co-author of 57 publications and inventor/co-inventor in 4 patents. He has received 4 awards for his research work, including the prestigious 2023 MNE Young Investigator and Lectureship Award. He is also co-founder of the spin-off company Nanoplasmas PC, which has received 2 VC rounds for the commercialization of LOC/microfluidic based devices for food, health and environmental applications.

1. Introduction

Rapidly widening water scarcity has sharpened interest in passive atmospheric water harvesting (AWH), where atmospheric water collection can offer alternative, low-energy, water supply pathways that can complement conventional infrastructure in arid and coastal regions.[1–4] Engineering progress has largely followed nature: directional capture, guided transport, and quick shedding inspired by beetle elytra, cactus spines, leaves, and spider silk have been emulated at multiple scales to improve both fog and dew collection, which stand as the two types of water source from air.[5–9] Reviews spanning materials, structures, and deployment underscore two recurring levers for performance: (i) stabilizing favorable wetting states to boost nucleation and suppress flooding,[10,11] and (ii) programming capillarity to drive coalesced drops toward collectors with minimal retention and re-evaporation.[12–14] In this context, it is important to distinguish between the two primary sources of atmospheric water, as their collection requirements differ fundamentally based on the physical state of the water. Fog consists of liquid water droplets suspended in the air; therefore, its collection is primarily a mechanical process dominated by droplet impact, capture, and shedding mobility. Conversely, dew refers to water in the gaseous vapor state that undergoes a phase change into liquid when it comes into contact with a surface cooled below the dew point. Consequently, dew harvesting efficiency is determined by a combination of nucleation site density, latent heat dissipation, and subsequent droplet drainage. Understanding these distinctions is crucial for designing surfaces that can effectively manage both airborne droplet capture and vapor phase-change cycles.[15]

In fog collection, early biomimetic surfaces coupled micro/nano-textures with wettability patterning to create capture–drain "circuits", such as hydrophilic islands or channels which can nucleate and coalesce droplets while adjacent hydrophobic textures minimize adhesion and speed shedding have been proposed.[15–17] Such approaches have been reported as surfaces which can significantly improve fog collection rates compared to surfaces with single wettability.[18] Recent research efforts have focused on fabrication techniques that allow precise control of biphilic patterns, such as lithography, laser structuring, plasma treatment, inkjet printing, and chemical patterning.[19–22] Channel-type designs ("capture & canalize") consistently outperform homogeneous meshes in guided transport regimes,[23,24] while gradient-Janus and hybrid-wettability films reduce pinning and shorten drainage paths.[25,26] Beyond topographic motifs, nonwoven and textile-based collectors leverage 3D porosity, large interfacial area, and multiscale roughness to enlarge capture cross-section and present low hydraulic resistance to departing droplets.[27,28] For example, a carbon-nanotube–coated nonwoven fabric inspired by the desert plant Salsola crassa, reported a fog yield of 2167 mg cm^{-2} h^{-1} (~520 L m^{-2} day^{-1}) by combining a Cassie–Baxter (hydrophobic) needle-punched face with a mildly hydrophilic carbon-nanotube–coated side and optimized fiber–fiber junctions—an explicit demonstration that wetting contrast and hierarchical porosity can be co-designed for very high throughputs.[29]

In dew collection, the controlling physics differ: yields are set primarily by nucleation sites density in combination with drop mobility which can be manipulated by controlling the surface chemistry and topography.[30,31] Whereas, the environmental conditions *e.g.* temperature difference between the sample and the environment (ΔT) and Relative Humidity (RH) are also critically affecting the water which is available for collection.[32,33] It has also been reported that filmwise condensation in atmospheric water collection (*i.e.* for humid air) can provide high water collection rates on superhydrophilic surfaces. Classic dewing studies established that dropwise condensation maximizes heat transfer and net yield relative to filmwise modes;[34] however, patterned "biphilic" surfaces (hydrophilic features on hydrophobic backgrounds) can further improve nucleation, without compromising the overall water mobility. It is therefore evident that literature in fog and dew collection includes several examples of biphilic surfaces with different biphilic area coverage to co-optimize nucleation and water collection.[35,36] For example, Hou *et al.*[37] introduced nanoscale-topography-based biphilicity to steer droplet self-organization and flow across hybrid wetting textures. Chehrghani *et al.*[38] theoretically/experimentally identified optimal hydrophobic-island sizes on superhydrophobic background for sustained dropwise flow condensation. Studies tuning the "active surface area" confirm that capture efficiency and drainage speed trade off with coverage; there is a finite window where coalescence is rapid yet films don't percolate.[39] Related biomimetic strategies implementing synergistic driving forces (Laplace, gravity, and Marangoni), superhydrophobic collectors augmented for initial capture,[40] and atmosphere-mediated, durable biphilicity on structured substrates can deliver measurable gains as much as 20% fog-harvesting improvement with scalable, abrasion-resistant patterning while addressing long-term durability needs.[41] Review papers and comparative experiments further emphasize that: (a) fog and dew reward different "best" designs because their limiting steps differ (capture rate *versus* heat-transfer-limited nucleation),[42] (b) transport geometry matters—spots *versus* stripes alter coalescence pathways, liquid bridges, and ejection mechanisms under otherwise identical chemistries[43] and (c) practical systems must integrate scalable patterning, mechanical robustness, and environmental compatibility (*e.g.*, low hysteresis superhydrophobic backgrounds with stable hydrophilic domains).[44–48] Finally, there are some recent interfacial heat-transfer and phase-change studies trying to map how patterned wettability modifies local condensation modes, transition to filmwise states, and shedding thresholds under variable flux, offering design rules that bridge lab setups and field conditions.[49–52]

Beyond liquid water collection, the engineering of biphilic surfaces is affected by research into condensation-frosting. It has been demonstrated that inter-droplet ice bridging (*i.e.* when a frozen droplet harvests water from neighboring supercooled liquid droplets to propagate across a surface) can be passively halted by using chemical micropatterns to spatially control nucleation sites. This spatial control is found to be pitch-dependent and perfect spatial control of condensation was observed for patterns with a pitch of 2, whereas larger pitches resulted in unintended nucleation on hydrophobic regions.[53]

Despite this progress, quantitative, side-by-side mapping of the effect of hydrophilic features size, shape (spots *vs.* stripes) and biphilic area coverage on a series of different micro-topographies (pillars, trapezoids, honeycombs) that can induce extreme wetting contrasts across both fog and dew regimes remains limited. Existing works often optimize a single pattern on a single topography (which in most times is random) or evaluate only one collection mode (fog or dew), making it hard to extract which biphilic pattern or combination of underlying topography and bihilic type is beneficial *versus* specific conditions. Moreover, from the fabrication point of view, many methods proposed are complex or involve the use of PFAS substances. Herein we try to fill this gap by fabricating a wide range of different PFAS-free, biphilic surfaces, *e.g.* superhydrophobic surfaces with hydrophilic spots with diameter of 500 μm and 1000 μm and superhydrophobic surfaces with hydrophilic stripes with width 1000 and spacing

1000 μm or 1000 width and 2000 μm spacing realized on three microtextures (pillars, trapezoids, honeycombs). Then these 12 different surfaces are benchmarked in both fog and dew performance under controlled RH–Δ*T* conditions. Specific topography design guidelines and biphilic patterns are demonstrated as more efficient and the underlying mechanism is also discussed.

2. Materials and methods

2.1. Fabrication of Si masters for soft lithography

For the fabrication of the ordered, superhydrophobic surfaces silicon masters with three different topographies (circular pillars, trapezoids and honeycombs) were realized utilizing lithography on silicon wafers followed by wet or dry etching. Si wafers were cleaned with piranha solution prior to the treatment. HMDS was deposited on the wafers (spin coating at 3000 rpm for 30 seconds) to improve the adhesion of the photoresist. The photoresist that is used in this work is the AZ 5214E, which was spin coated on the wafers at 3000 rpm for 30 seconds, resulting in a thickness of 1.5 μm. Next, the wafers were thermal treated at 95 °C for 10 minutes. For the three patterns fabricated, quartz masks were designed and purchased (Fig. 1a–c). For the exposure a Karl Suss MA6 mask aligner was used, which allows for vacuum contact. The exposure duration was 70 seconds at 320 nm wavelength. For the removal of the exposed photoresist developer 726 MIF was used and the development lasted 1 minute, followed by thermal curing at 120 °C for 15 minutes. Images of the patterns created on the Si wafers after the optical lithography step are provided in Fig. 1(d) and (e). For the pattern transfer of the posts and the holes patterns plasma etching (Bosch process) was used.

The Bosch process was performed using an Alcatel MET ICP plasma reactor. The process alternated between a deposition step and an etching step. During the deposition phase, C_4F_8 gas was introduced at a flow rate of 105 sccm for 3 seconds. This was followed by the etching phase, where SF_6 gas was flowed at 170 sccm for 6 seconds. The reactor operated with a source power of 1900 W and a bias power of 150 W, while the chamber pressure was maintained at 45 mTorr. Throughout the process, the sample temperature was held constant at 20 °C. The process lasted for 5 minutes for the large circular pillars and 2 minutes for the small circular holes. In Fig. 2 are presented SEM images of the Si masters after the bosch etching. Fig. 2a shows Large circular pillars after etching for 5 minutes. Fig. 2b shows the small circular holes etched for 2 minutes.

For the trapezoidal structures, first 200 nm of silicon oxide was developed on the wafers *via* thermal oxidation at 1100 °C for 140 minutes using a TEMPRESS oven to enhnance adhesion of the nitride which will be deposited. Then, a 200 nm layer of nitride was deposited on the wafers using chemical vapor deposition at 800 °C for 30 minutes. After the nitride deposition, the same process of optical lithography was used, HMDS was deposited on the wafers, followed by the AZ

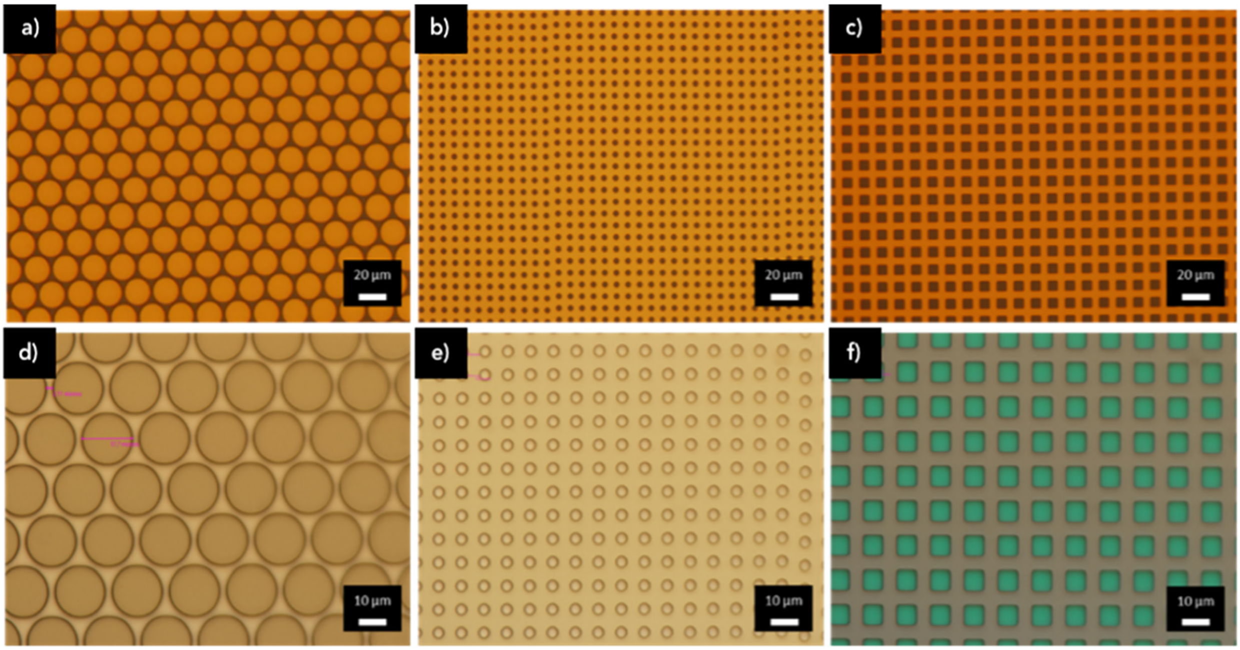

Fig. 1 (a)–(c) Images from optical microscope of the quartz masks for (a) 18 μm wide circular pillars in hexagonal formation, which will provide honeycomb cavities on PDMS, (b) 5 μm wide circular holes in which will provide cylindrical pillars on PDMS, (c) 5 μm wide square holes which will provide trapezoids on PDMS. (d) 18 μm wide circular pillars in hexagonal formation (Si master), which will provide honeycomb cavities on PDMS, (e) 5 μm wide circular holes (Si master), which will provide cylindrical pillars on PDMS, (f) 5 μm wide square holes (Si master), which will provide trapezoids on PDMS.

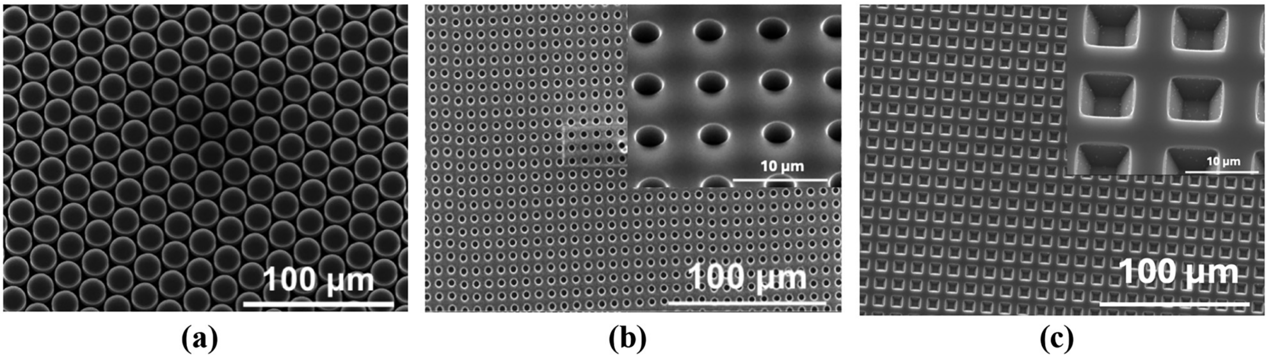

Fig. 2 SEM images of the Si master for (a) large circular pillars (diameter is 18 μm and the depth 15 μm) (b) small circular holes (diameter is 5 μm and the depth 5 μm) (c) trapezoids (square width is 7 μm and the depth 4 μm).

5214E. Next, the wafers were cured at 95 °C for 10 minutes and the exposure lasted 70 seconds at 320 nm wavelength. For the removal of the exposed photoresist again developer 726 MIF was used, the development lasted 1 minute, followed by curing at 120 °C for 15 minutes. For the pattern transfer to the nitride, SF_6 plasma etching was used for 5 minutes followed by immersion in BHF for 1 minute (to remove the last layer of the oxide smoothly). Finally, the wafers were cleansed with acetone and propanol to remove the remaining photoresist. For the formation of trapezoid holes, the square patterned silicon wafers were subjected to silicon crystallographic etching, using KOH solution. The set up consists of a vessel that contains the KOH solution, immersed in a bath of oil, that contains heating coils for the temperature control, and 3 beakers, 1 with 1% HF solution, and 2 with DI water, for the removal of the natural silicon oxide. The KOH solution concentration was 40% and the temperature was set at 60 °C, these parameters correspond to an etching rate of about 450 nm min^{-1}. The wafers were immersed in the 3 beakers and then immediately immersed in the KOH bath, followed again by immersion in water for the removal of the solution. Etching time was set to 10 minutes and the resulting Si master was characterized using optical profilometry.

In Fig. 2, the scanning electron microscopy (SEM) images of the three Si masters are provided. Three-dimensional optical profilometry maps and the corresponding line profiles are provided in the SI. On the large circular pillars diameter is 18 μm and the depth 15 μm, on the small circular holes diameter is 5 μm and the depth 5 μm and on the square width is 7 μm and the depth 4 μm.

2.2. Design and fabrication of superhydrophobic and biphilic surfaces

For the pattern transfer of the master topography, we used the soft lithography using Polydimethylsiloxane PDMS which also provides flexibility. Polydimethylsiloxane (PDMS) prepolymer was prepared by combining the base and curing agent (10 : 1 w/w) and mixing until homogeneous. The mixture was degassed under vacuum to remove entrained air, dispensed onto the different stamps, and spin-coated (at 580 rpm for 60 s) to fill the relief features, resulting in a thickness of 200 μm; a brief second degassing minimized trapped bubbles. The coated stamp was then thermally cured on a hot plate (80 °C, until fully cross-linked) and allowed to cool to room temperature. Finally, the PDMS was gently demolded to obtain an accurate replica of the Si master microstructure. Samples for fog collection, were prepared as square plates measuring 2 cm × 2 cm with a thickness of 2 mm and for dew collection PDMS samples were square plates measuring 4 cm × 4 cm with a thickness of 0.2 mm. The complete process is shown in SI.

A total of four different stencil masks were designed to create superhydrophilic patterns on the superhydrophobic PDMS substrates. Two types of biphilic patterns (spots and stripes) with different geometrical characteristics were prepared to study the effects of pattern design on water collection efficiency. The masks were designed in AutoCAD and fabricated by drilling or milling with the use of micromilling machine (LPKF protomat E44) on 1 mm thick PMMA sheets to ensure accurate dimensions and pattern fidelity. The schematic representation of the process to develop the biphilic surfaces is shown below (Fig. 3a). Prior to use, all stencils were thoroughly cleaned with ethanol to remove any contaminants. Each stencil was carefully aligned and placed in direct contact with the PDMS substrates. Alignment was crucial to ensure that the superhydrophilic patterns were accurately transferred according to the designed geometries. Stencils were secured in place using adhesive tapes at the edges, avoiding interference with the coating area. The designs realized are: Pattern 1: uniform array of circular spots (spot diameter 500 μm and 400 μm spacing, Fig. 3b). Pattern 2: uniform array of circular spots (spot diameter 1000 μm and 800 μm spacing, Fig. 3c). This design enables the evaluation of the effect of spot size on fog and dew collection. For the creation of stripes, channels were engraved on the PMMA. Pattern 3: stripes of 1000 μm width and 1000 μm spacing (Fig. 3d). Pattern 4: stripes of 1000 μm width and 2000 μm spacing (Fig. 3e). This design aimed to investigate the influence of line width and spacing on directional water transport during fog and dew collection. The hydrophilic coverage for each mask is the following 25% for both circular-spot designs (500 μm and 1000 μm), 50% for

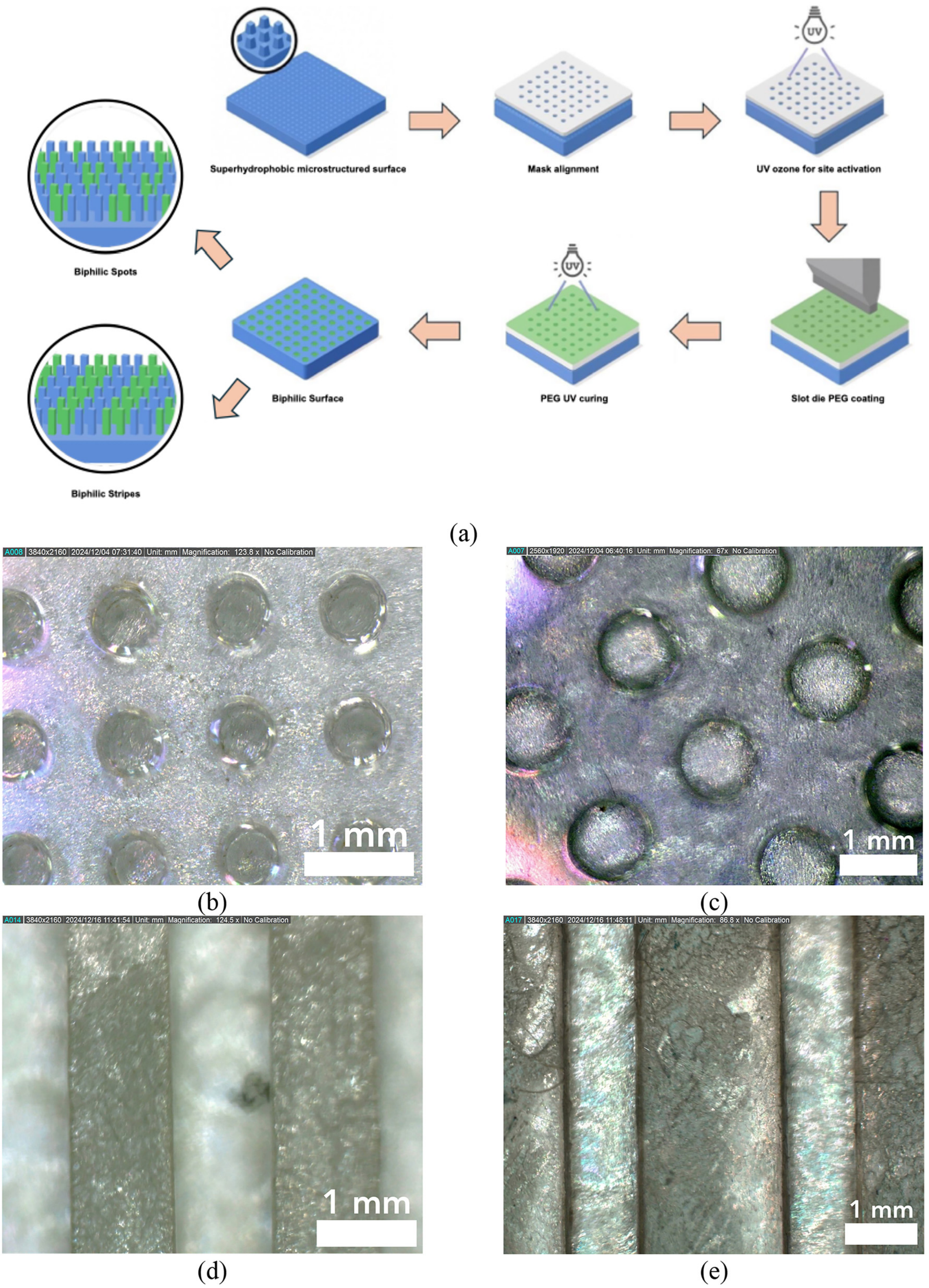

Fig. 3 (a) Schematic representation of the process to fabricate biphilic surfaces, with blue the hydrophobic areas and with green the hydrophilic domains created using the stencil slot-die coating process are shown. Optical microscope images of the stencils that are used for the biphilic patterning: (b) spots of 500 μm diameter and 400 μm spacing (25% hydrophilic coverage), (c) spots of 1000 μm diameter, 800 μm spacing (25% hydrophilic coverage), (d) stripes of 1000 μm width and 1000 μm spacing (50% hydrophilic coverage), (e) stripes of 1000 μm width and 2000 μm spacing (35% hydrophilic coverage).

1000 : 1000 μm stripes, and 35% for 1000 : 2000 μm stripes. In this way except from the pattern type the biphilic ratio will be also evaluated.

Then, PEG 8000 (10% w/v) was used to create the four different superhydrophilic pattenrs on the masked substrates. Ossila slot die coater was used to apply the PEG 8000 solution. The coating parameters used are: coater shim: 0.1 mm thickness, bed temperature: 100 °C, coating length: 70 mm, coating speed: 5008 mm s^{-1}, dispense rate: 20 137 μl s^{-1}, stage delay: 0. After coating, the substrates were placed under a UV light source emitting at 365 nm. Samples were exposed for 2 hours to ensure complete cross-linking and adhesion of the PEG8000 coating. The extended exposure time was selected based on preliminary tests indicating optimal curing conditions for the PEG 8000 layer. After UV exposure, the substrates were allowed to sit for an additional 1 hour at room temperature. This step ensured that the PEG8000 coating was fully set and any residual moisture had evaporated.

2.5. Fog collection setup

The experiment utilizes a 11 L plastic container which is filled with 2 L of DI water, ensuring the ultrasonic mist makers are fully submerged. A 9 L, 550 W oil free compressor, positioned on the container's lid, facilitates the airflow necessary for directing fog through a nozzle at a constant speed of 3.3 m s^{-1}. Positioned 10 cm from the nozzle, a metal sample holder, directly facing the fog flow, supports the sample collection with a beaker placed beneath to gather the water. Every 15 minutes, water collection is quantitatively measured using a precise 4-digit scale over a duration of 45 to 60 minutes. All measurements were repeated three times per tested surface to ensure reproducibility. In total 3 different surfaces were evaluated and the average water collection rate and standard deviation were extracted.

2.6. Dew collection setup

Dew collection experiments were performed in a sealed transparent chamber (30 × 10 × 15 cm) with controlled humidity and temperature. A Peltier thermoelectric cooling module was used to cool the test surfaces, generating a surface-to-air temperature difference (ΔT) of 5 °C or 15 °C. The chamber humidity was set to either 70% or 90% using an ultrasonic humidifier connected through a regulated airflow line. Each 4 × 4 cm surface was placed horizontally on the cooled stage, with a thermocouple attached to monitor temperature. Dew condensed directly onto the exposed surface as it cooled below the dew point. The collected water was measured using a precision balance at regular time intervals over a 90-minute collection period. All measurements were repeated three times per tested surface to ensure reproducibility. In total 3 different surfaces were evaluated and the average water collection rate and standard deviation were extracted. This setup enables a controlled comparison of dew harvesting efficiency between biphilic surfaces under well-defined environmental conditions. (The images and the detailed description of the experimental configurations used for the evaluation of fog and dew collection are provided in section S3 of the SI.)

2.7. Video analysis of drop formation, growth and removal

To investigate the physical mechanisms governing the water collection performance of surfaces with different micro-topographies, *in situ* dynamic droplet video tracking was conducted. Videos were recorded at 120 or 240 fps. Specifically, the dimensions of the ten largest droplets on each surface were measured at 10 seconds intervals, allowing for the precise extraction of the time-dependent evolution of the mean droplet diameter up to the point of droplet departure. For the drop size analysis Image J software was used.

3. Results and discussion

3.1. Surface morphology

The pattern transfer on the PDMS was evaluated using SEM imaging as well as white light interferometry (Fig. 4). The three different topography types (pillars, trapezoids and honeycombs) were designed to provide a superhydrophobic state with apparent contact angle higher than 150° following Cassie–Baxter equation. To this end, f_s (solid–liquid area fraction) is close to 0.2 for all three types of topographies. However, these topographies exhibit different geometrical characteristics and are expected to exhibit different performance in atmospheric water collection. For example, the honeycomb type surfaces exhibit large and relatively deep cavities, whereas the trapezoid type surfaces can enable an upwards Laplace pressure gradient, which can be beneficial in atmospheric water collection.[54] Finally, the pillar type surface is a typical ordered topography used for superhydrophobicity.

3.2. Wetting properties

To systematically investigate the influence of topographical and chemical patterning on atmospheric water harvesting, a comprehensive matrix of twelve distinct biphilic designs was engineered. To ensure robust macroscopic validation and account for physical fabrication variance, three independent replicate surfaces were fabricated for each design, yielding a total library of 36 distinct testing samples. Three distinct microstructured substrates were employed as the superhydrophobic background: pillars (consisting of vertical cylindrical pillars with a height of approximately 5 μm and a diameter of 5.5 μm), honeycombs (characterized by a honeycomb-like structure with a 15 μm height and 18 μm diameter), and trapezoids (featuring trapezoid-like features with a height of 4 μm and a large base surface area of approx.7 × 7 μm). On top of each substrate, four different superhydrophilic pattern geometries were applied to create contrasting wetting regions: circular spots with diameters of 500 μm and 1000 μm, and stripe patterns with dimensions of 1000 : 1000 μm and 1000 : 2000 μm (hydrophilic : hydrophobic). This combination of surface topographies and pattern geometries resulted in twelve unique biphilic configurations that enable a systematic

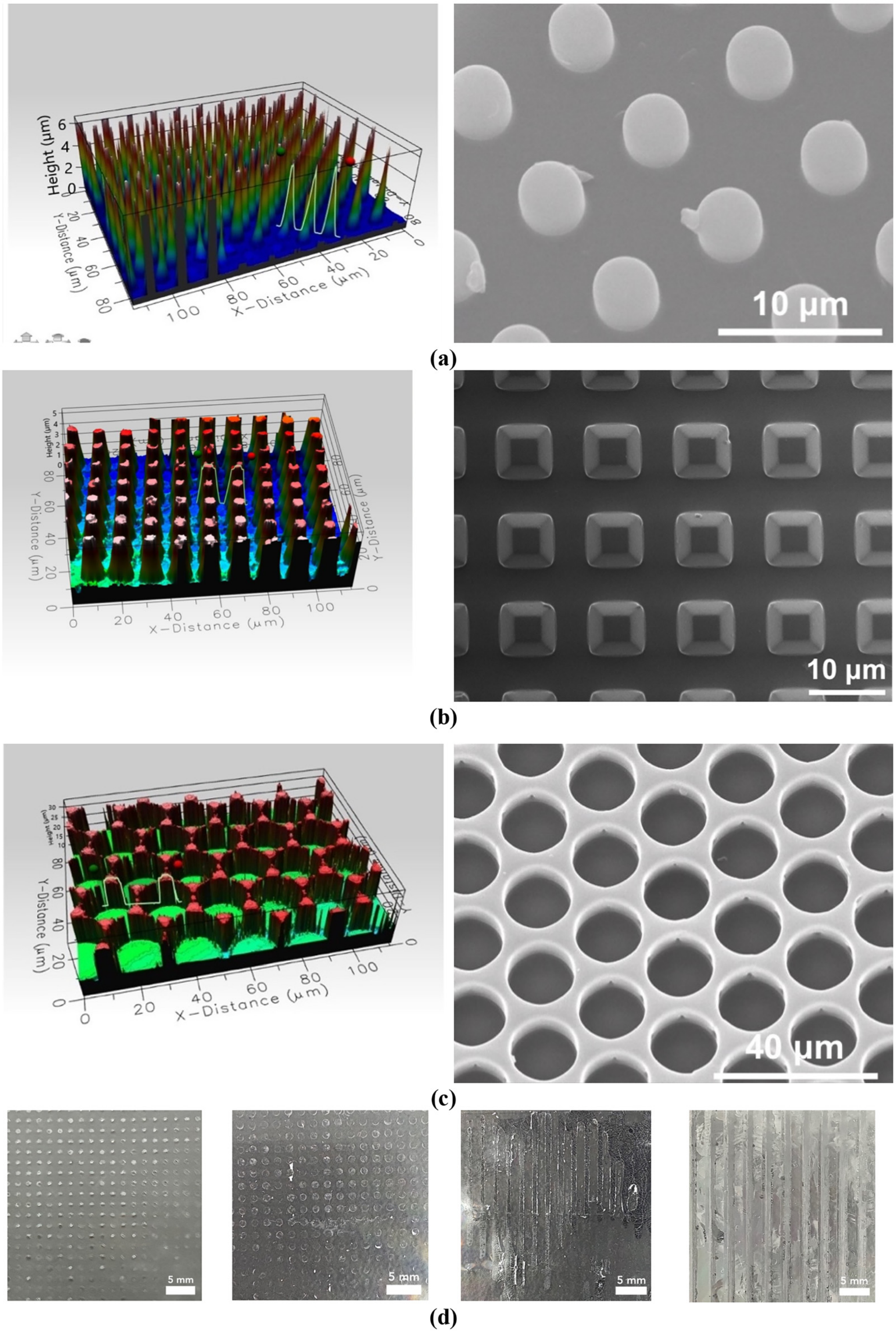

Fig. 4 SEM images of the three deterministic topographies fabricated by PDMS soft lithography to enable the realization of superhydrophobic surfaces and their respective surface topography analysis using optical interferometry for (a) pillar-type structures (b) trapezoid-type structures (c) honeycomb-type structures (d) representative images of the 4 different biphilic surfaces (left to right spots 500 μm, 1000 μm, stripes 1000 : 1000 μm, stripes 1000 : 2000 μm).

evaluation of pattern size, shape and biphilic ratio in fog and dew collection performance. The static water contact angle (WCA) and contact angle hysteresis (CAH) for the superhydrophobic and superhydrophilic areas of each substrate are summarized in Table 1, illustrating the strong wetting contrast between the two regions.

3.3. Drop formation evaluation and biphilic surfaces working principle

As observed in the resulting kinetic profiles, the micro-structured topographies accelerated both droplet coalescence and the overall shedding frequency relative to the untreated PDMS. On the structured pillar and trapezoid surfaces, captured droplets exhibited highly dynamic growth, rapidly coalescing to reach critical departure diameters of 3.22 mm and 3.19 mm at just 140 seconds and 150 seconds, respectively. Upon reaching this critical size threshold, the droplets shed immediately, mechanically demonstrating a highly mobile, low-adhesion Cassie–Baxter wetting state (Fig. 5). In contrast, droplets on the flat and untreated PDMS surface, exhibited delayed coalescence and severe capillary pinning. At t = 140 seconds, the exact time at which the pillar arrays were already initiating macro-shedding events, the droplets pinned on the flat PDMS had only reached an average diameter of 1.6 mm. Consequently, the untreated PDMS required a severely prolonged residence time (~300 seconds) and much higher departure diameter (>4 mm) to overcome the adhesion force of the PDMS surface (Fig. 5).

More interestingly, the honeycomb topography exhibited severe pinning of the drops in the micro-cavities and transitioned into a flooded Wenzel state. This resulted in the formation of elongated liquid films that cleared only once every 10 minutes, thereby providing a mechanistic explanation for the significantly lower collection efficiency which is observed in the next sections in both modes of water collection. Videos for all surfaces are provided as SI.

Moving now on the working principle of the biphilic patterns. On the stripe configurations, water removal operates through a highly efficient, continuous five-stage cycle as shown in Fig. 6. During Stage 1 (nucleation and growth), micro-droplets nucleate and continuously grow *via* coalescence on the superhydrophobic runway, maintaining a highly spherical shape due to low surface adhesion. In Stage 2 (boundary interception), the droplets reach their critical departure diameter and make physical contact with the chemical boundary of the adjacent superhydrophilic stripe. This triggers Stage 3 (capillary migration), where strong capillary forces from the superhydrophilic domain actively draw the droplet off the hydrophobic lane, initiating rapid directional transport. During Stage 4 (complete surface clearing), the droplet is fully

Table 1 Water contact angle (WCA) and contact angle hysteresis (CAH) measurements on the biphilic surfaces

	Hydrophobic/superhydrophobicareas		hydrophilic/superhydrophilic areas
Substrate	WCA	CAH	WCA
Pillars	162° 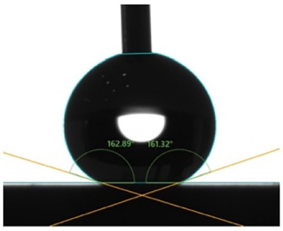 	9°	20° 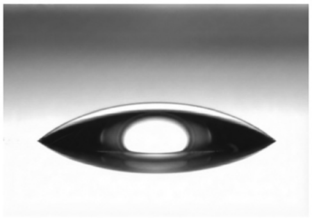
Trapezoids	145° 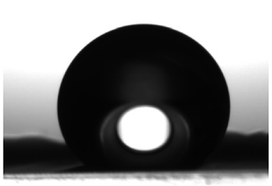	>45°	17° 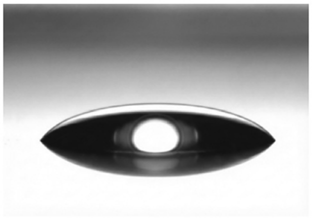
Honeycombs	140° 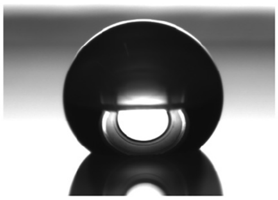	40°	16° 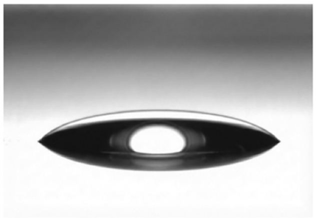

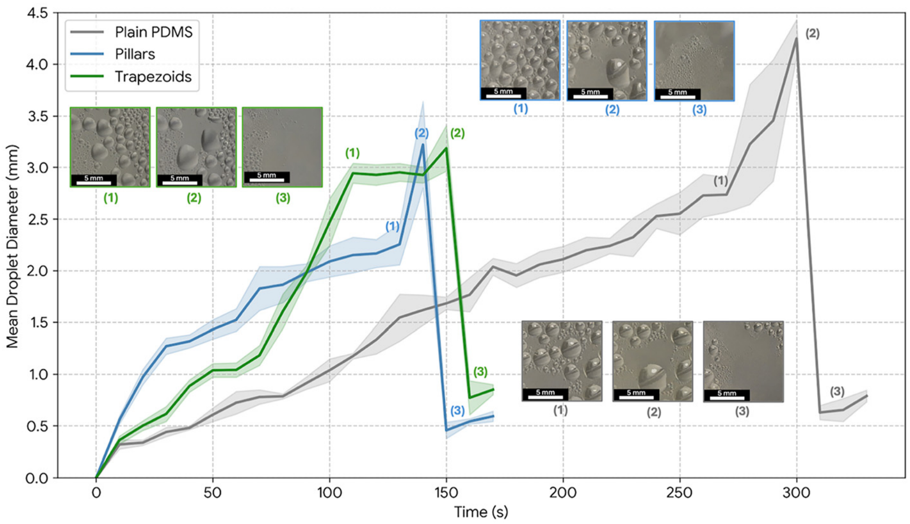

Fig. 5 Time evolution of the mean size of the 10 largest droplets on each surface during fog collection. Representative optical images are provided to visually capture the critical progression of the collection cycle on each surface, specifically highlighting localized nucleation, continuous droplet growth into a single critical mass, and subsequent shedding.

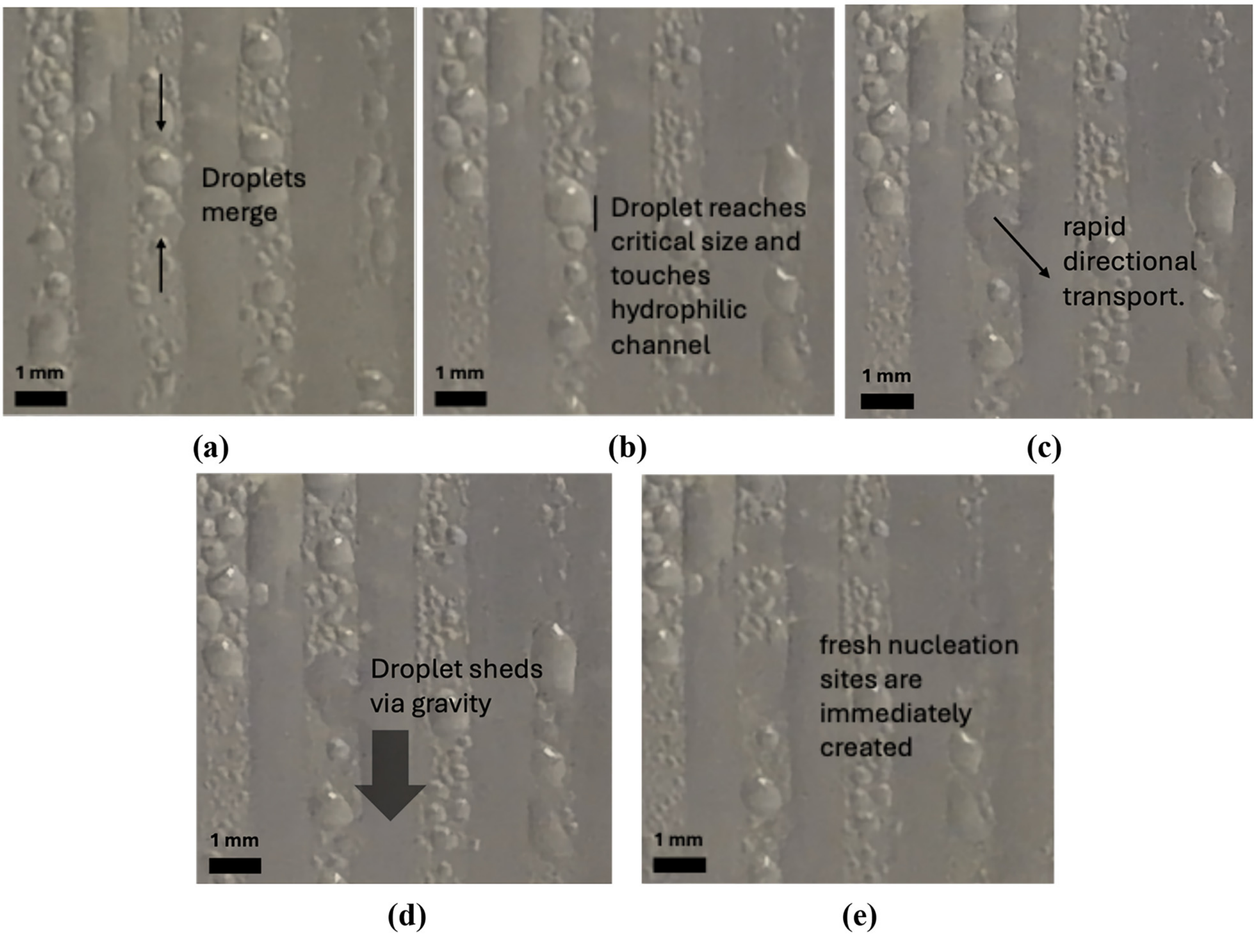

Fig. 6 Time-lapse optical images illustrating the five-stage capillary-driven droplet removal mechanism on the biphilic stripe patterns during fog harvesting. (a) Nucleation and highly spherical growth on the superhydrophobic runway. (b) Boundary interception as the droplet reaches its critical departure diameter. (c) Capillary migration initiated by the adjacent superhydrophilic domain. (d) Complete surface clearing as the droplet transfers into the hydrophilic reservoir and sheds *via* gravity. (e) Cycle renewal, exposing the dry hydrophobic runway for subsequent fog capture.

transferred into the hydrophilic channel and subsequently sheds *via* gravity, leaving the superhydrophobic runway empty and ready for Stage 5 (cycle renewal), in which the cleared hydrophobic runway immediately exposes fresh nucleation sites, preventing generalized filmwise condensation and restarting the high-efficiency collection cycle.

On the other hand, the discrete biphilic spot patterns operate through a mechanism of geometric confinement, which was documented in a three-stage visual sequence (Fig. 7). Initially, micro-droplets are formed and start to accumulate on the localized superhydrophilic capture points. As time passes, these droplets grow and coalesce to create larger, localized liquid formations with an average size of 3 mm. While these formations deviate from ideal spherical droplets due to the high-adhesion pinning of the spots, the physical separation provided by the highly repellent superhydrophobic background effectively arrests extensive liquid bridging. This confinement actively stops the formation of the continuous, macroscopic water films that were observed completely flooding the stripe patterns. Finally, once these discrete 3 mm formations reach their critical mass, gravity overcomes the localized pinning forces, rapidly removing the liquid and leaving the area completely open for cycle renewal. Live video analysis determined that this discrete growth and shedding process operates on a consistent cycle, averaging 2 minutes and 40 seconds. Again, videos for both types of biphilic surfaces are provided as SI.

3.4. Fog collection results

Fog harvesting was measured as water collection rate (WCR) using a fog flow of 3.3 m s^{-1} and the sample was placed at a distance of 10 cm from the fog outlet. Fig. 8 compiles the results for all twelve biphilic combinations together with a flat hydrophobic PDMS sample as reference. The flat PDMS reference sample exhibited an average WCR: 4.01 ± 0.76 g cm^{-2} h^{-1}. Among the three micro-structured substrates with one type of wettability, the surface with the highest WCA and lower CAH (*i.e.* pillars) which exhibits inherently high droplet mobility achieves the highest baseline in WCR reaching 4.39 g cm^{-2} h^{-1}, significantly higher compared to flat PDMS (the performance of the hydrophobic and superhydrophobic surfaces in fog collection is provided in the SI).

The primary factor governing fog harvesting is droplet mobility. Because fog collection is dominated by flow-driven droplet impact, efficient harvesting requires rapid removal of droplets immediately after they land on the surface. Surfaces that minimize pinning and enable directional drainage are expected to perform better. To this end, wettability is expected to critically affect WCR. Biphilicity can be beneficial by providing extra capturing points, but increased biphilic ratio can delay droplet shedding, particularly on topographies that already exhibit high mobility. Interestingly, all biphilic patterns tested with biphilic surface coverage from 25 to 50% reduced WCR by approximately 11–30%. This indicates that, on surfaces where droplet shedding is already efficient, additional hydrophilic regions can impede drainage rather than enhance capture. For pillar substrates, all four biphilic designs produced fog yields within a narrow range. The surfaces patterned with 500 μm spots, 1000 μm spots, 1 : 1 stripes, and 1 : 2 stripes collected 3.86 ± 0.32, 3.72 ± 0.69, 3.66 ± 0.55, and 3.76 ± 0.48 g cm^{-2} h^{-1}, respectively. The best-performing configuration (500 μm spots) remained only 3.6% below the flat hydrophobic PDMS reference sample, and in all other patterns WCR decreased by 6–9%. These results suggest that once a substrate already exhibits high droplet mobility, the detailed geometry of the biphilic pattern has only marginal influence on fog collection. Trapezoidal surfaces show a slightly broader spread in performance across patterns. The surface with 1000 μm spots collected 3.81 ± 0.64 g cm^{-2} h^{-1}, approximately 5% below the PDMS reference. The remaining biphilic variants —500 μm spots, 1 : 1 stripes, and 1 : 2 stripes—yielded 3.25 ± 0.53, 3.46 ± 0.59, and 3.00 ± 0.52 g cm^{-2} h^{-1}, corresponding to

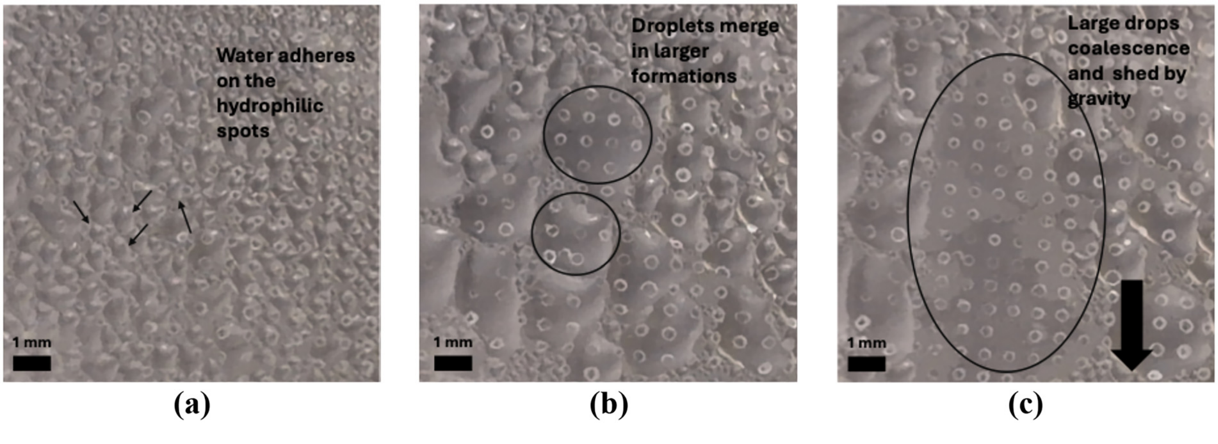

Fig. 7 Time-lapse visualization of the discrete droplet growth and removal cycle on the biphilic spot patterns during fog harvesting. (a) Initial nucleation and accumulation of micro-droplets on the superhydrophilic capture points. (b) Coalescence into larger, discrete liquid formations (averaging 3 mm in size). The superhydrophobic background geometrically confines the water, actively preventing the formation of a continuous, flooded film. (c) Rapid, gravity-driven removal of the liquid formation once critical mass is reached, leaving the surface completely open for cycle renewal. This complete clearing cycle operates at an average frequency of 160 seconds (2 min 40 s).

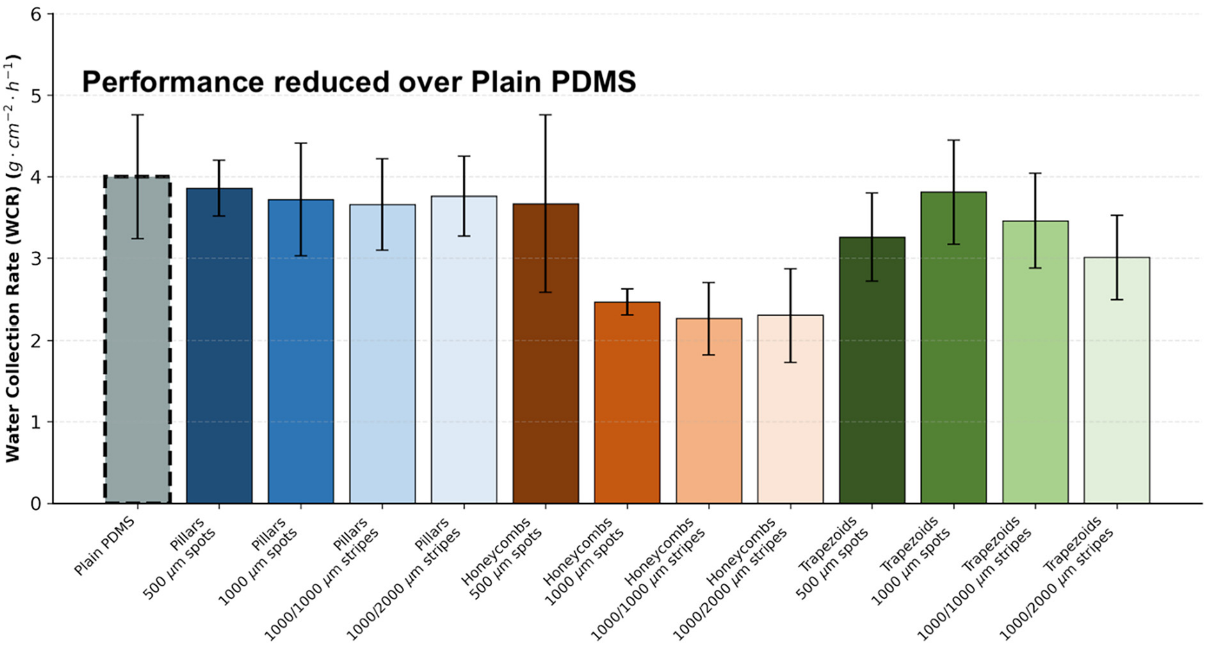

Fig. 8 Fog collection performance of biphilic surfaces with different biphilic patterns on surfaces with pillar, honeycomb, and trapezoid microstructures.

reductions of 19%, 13%, and 25%, respectively. Larger circular spots appear better suited than stripes for this topography, likely due to their ability to act as capturing points without compromising droplet mobility to the degree that stripes affect it (biphilic ratio is 25% compared to higher biphilic ratios for the stripes 35–50%).

Honeycomb substrates suffer from intrinsically low droplet mobility and strong retention within the cavities. The larger interspace distance for this topography is significantly larger compared to the other two and drops pin and don't jump upon coalescence. In this topography, hydrophilic patterning significantly improves performance. The honeycomb surface collects only 2.01 ± 0.90 g cm^{-2} h^{-1}, but this value increases to 3.67 ± 1.08 g cm^{-2} h^{-1} when patterned with 500 μm spots, representing an 83% improvement. The surfaces patterned with 1000 μm spots, 1 : 1 stripes, and 1 : 2 stripes collect 2.45 ± 0.16, 2.26 ± 0.43, and 2.29 ± 0.57 g cm^{-2} h^{-1}, corresponding to gains of 22%, 13%, and 14%, respectively. Nevertheless, even with these enhancements, the WCR in all honeycomb-based designs remain significantly lower compared to the PDMS reference sample (between 8% and 44%), indicating that biphilicity improves performance, but cannot completely eliminate the limitations imposed by the honeycomb geometry.

Overall, these results highlight that droplet mobility is the dominant mechanism in fog harvesting. For surfaces with inherently good shedding such as pillars, hydrophilic coverage should be kept minimal (<25%), and small circular spots are preferred. For retention-prone geometries such as honeycombs, moderate coverage with dense arrays of small hydrophilic spots can provide the greatest gain.

3.5. Dew collection results

Each surface consisted of a hydrophobic and superhydrophobic microstructured topographies fabricated in the form of pillars (5.5 μm height), honeycombs (15 μm height), or square-based trapezoids (4 μm height) combined with patterned hydrophilic regions in the form of circular spots or linear stripes (500 μm spots, 1000 μm spots, 1000 : 1000 μm stripes, and 1000 : 2000 μm stripes). Dew collection efficiency was evaluated under three representative environmental conditions: (i) 70% RH/ΔT = 15 °C, (ii) 90% RH/ΔT = 15 °C, and (iii) 90% RH/ΔT = 5 °C. The results are reported as mean water-collection rate (WCR, g cm^{-2} h^{-1}) and as percentage gain relative to the plain PDMS surface used as reference in Fig. 9a–c.

Unlike fog harvesting, in which droplet mobility is the dominant factor, dew collection is a phase change phenomenon, which depends on both droplet mobility as well as in nucleation sites density, which determine the nucleation rate.[55] Nucleation sites density is affected by surface properties like topography and wettability, since: (a) specially engineered patterns, can manipulate nucleation density and can enable control on how droplets are formed and behave during condensation cycles. (b) Hydrophilic areas can form more hydrogen bonds and attract vapor molecules. Thus, to improve dew collection, optimization of both droplet mobility as well as nucleation sites density is required. The flat PDMS reference sample yielded 0.0163 ± 0.0033 g cm^{-2} h^{-1} at 70% relative humidity and ΔT = 15 °C, 0.0317 ± 0.0058 at 90% RH and ΔT = 5 °C, and 0.0467 ± 0.0153 at 90% RH and ΔT = 15 °C. As expected, increasing humidity and temperature difference led to higher absolute water collection rates.

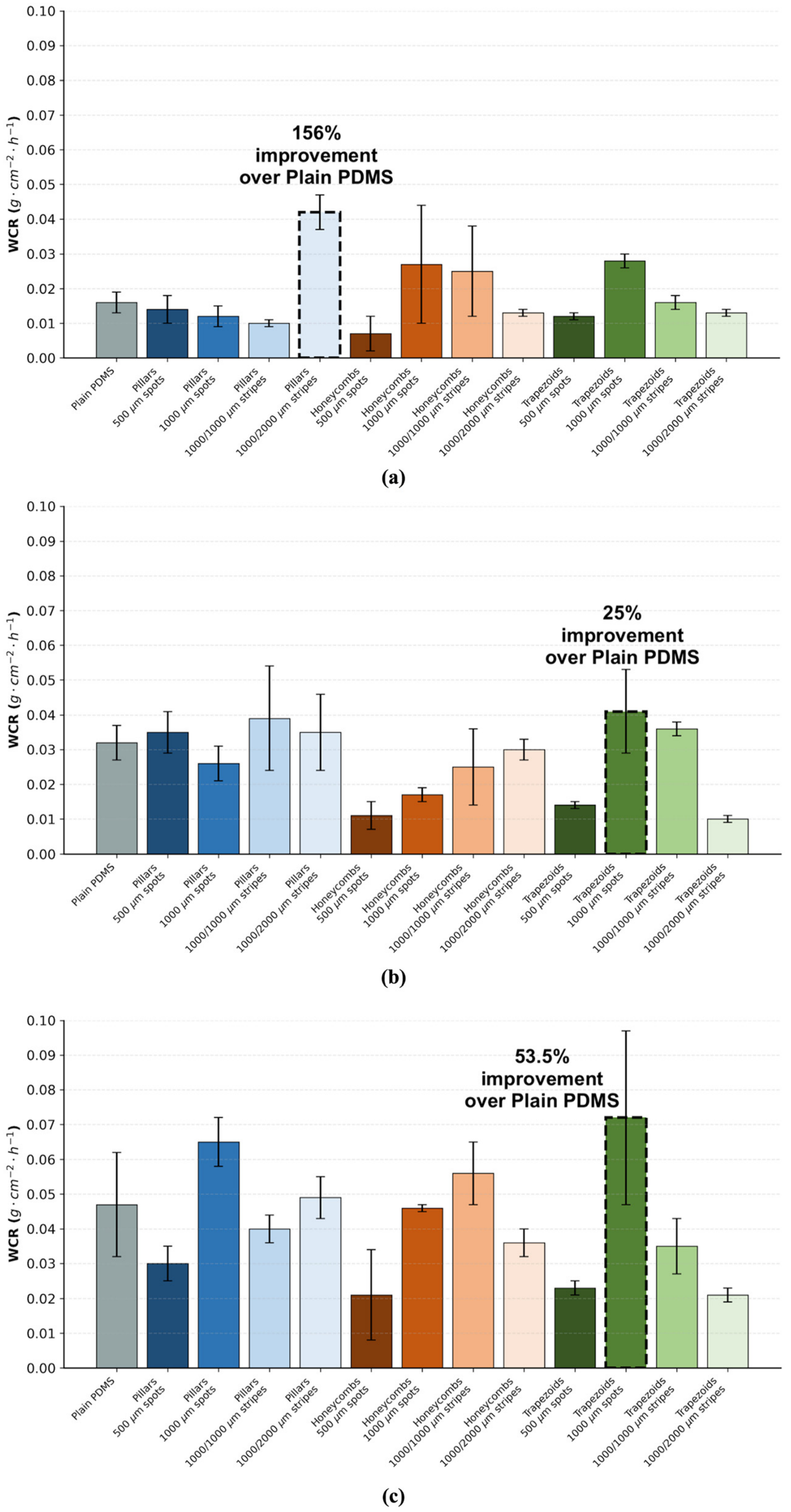

(a)

(b)

(c)

Fig. 9 Water collection rate in dew collection for all the 12 different types of biphilic surfaces when tested in three different environmental conditions (a) relative humidity of 70% and temperature difference of 15 °C (b) relative humidity of 90% and temperature difference of 5 °C (c) relative humidity of 90% and temperature difference of 15 °C.

Under intermediate humidity conditions (70% RH and $\Delta T = 15$ °C) (Fig. 9a), the most effective design combined pillar microstructures with parallel hydrophilic stripes $W = 1000 : S = 2000$ μm. This surface collected 0.0417 ± 0.0050 g cm^{-2} h^{-1}—a 156% improvement over flat PDMS. In this regime, where both nucleation and drainage are moderate, the introduction of stripes plays a critical role. The hydrophilic stripes promote nucleation and coalescence in the hydrophilic areas and then gravity in combination with the stripes provide directional drainage, while the remaining superhydrophobic areas supports fast droplet removal. According to calculations done in a previous work,[40] the film on the superhydrophilic area will grow to a thickness of approximately 150–200 μm, and then water will slide with an average velocity of 0.1 ms^{-1}, thus the effect of the poor mobility on superhydrophilic areas is reduced. Hydrophilic coverage also plays a central role in water collection performance. At these conditions (70% RH and $\Delta T = 15$ °C), the best-performing surface (pillars with 1000 : 2000 μm stripes) featured 35% hydrophilic coverage. This configuration outperformed PDMS by balancing drainage pathways with a sufficient superhydrophobic "runway" (65% of the total area) to sustain rapid water collection. Increasing hydrophilic area further (*e.g.*, 50% stripes) reduced effectiveness by suppressing mobility. Biphilic spot patterns at 70% RH and $\Delta T \approx 15$ °C, neither spot size on pillars outperformed the stripe-based optimum, and trapezoids again preferred 1000 μm (0.0285 *vs.* 0.0120).

At high humidity levels (90% RH) and significantly lower temperature difference ($\Delta T = 5$ °C) (Fig. 9b), the pillar structures with 1000 : 1000 stripes, trapezoids with 1000 μm spots and trapezoids with 1000 : 1000 stripes exhibited the highest WCR, achieving 0.039, 0.0408 and 0.0363 g cm^{-2} h^{-1} representing a WCR improvement over 25% compared to PDMS. Here, the benefit is more modest but still evident, driven mainly by the high biphilic area coverage which in two of the best performing surfaces is 50%. Recent literature also suggests that filmwise condensation is better in atmospheric water harvesting, since nucleation rate on superhydrophilic surfaces is significantly higher compared to superhydrophobic, whereas the conduction thermal resistance can be negligible, enabling condensation which is driven by diffusion and drainage rates.[34]

At high humidity conditions (90% RH) and $\Delta T = 15$ °C (Fig. 9c), in which the water content of the vapor is significantly higher, the highest performance was achieved with 1000 μm hydrophilic spots, yielding a WCR of 0.0717 g cm^{-2} h^{-1} (on trapezoids) and WCR 0.065 g cm^{-2} h^{-1} (on pillars), which is translated to a 53.5% and 39% gain over the PDMS reference. The improvement arises from the increased nucleation sites density on the hydrophilic spots without promoting early film formation and without compromising the overall water mobility of the surfaces, since biphilic area coverage for this biphilic design is low (25%). Moreover, it is also evident that the critical departure diameter (D_c) is also a critical factor. The WCR results at high humidity (90% RH) and $\Delta T = 15$ °C clearly show that when vapor content is high, this can lead to rapid droplet growth and the 1000 μm spots act as larger 'capillary reservoirs', which enable the growth of larger drops on the hydrophilic areas outperforming the 500 μm variants, despite the fact that on the smaller 500 μm spots critical departure diameter is expected to be lower (yielding 0.0717 *vs.* 0.0230 g cm^{-2} h^{-1} on trapezoids).

The results presented indicate that there is no universally optimal geometry, but clear strategies emerge for different regimes. When water content in the vapor is low, as in the ambient-like, intermediate conditions 70% RH/$\Delta T = 15$ °C case, protrusion type topographies such as the pillar textures with biphilic stripes are preferred. On the contrary on adverse conditions (higher humidity ratio and ΔT) low biphilic surface coverage is preferred and large spots (*i.e.* 1000 μm) are performing better. These observations reinforce the trade-off: increasing hydrophilic coverage can open drainage pathways and trigger nucleation, but too much coverage reduces mobility and overall throughput. Spot diameter also plays an important role, even at constant hydrophilic coverage (25%). Reducing spot size from 1000 μm to 500 μm increases the number of islands and doubles the hydrophilic–hydrophobic boundary per unit area. However, the effect is regime- and topography-dependent. At 90% RH and $\Delta T = 15$ °C, larger spots consistently outperform smaller ones. On trapezoids,

Table 2 Comparison of dew collection performance with state-of-the-art biphilic surfaces

Surface design	Collection mode	Green (PFAS-free)	WCR (g cm^{-2} h^{-1})	Ref.
PTFE nanoparticles on PIB rubber	Dew	No	0.072	31
Nanolaser hydrophilic patterns on aluminum	Dew	No	0.01	11
Biphilic nanoscale topography (hydrophilic nylon-CNT nanobumps)	Dew	No	0.095	37
Substrate: AlSi coating: liquid-like polymer	Fog & dew	Yes	3.06 (fog) 0.055 (dew)	48
Square biphilic patterns (hydrophilic alumina spots on superhydrophobic HDFS)	Fog	No.	2.05	39
Hydrophilic copper-epoxy spots	Fog	Yes	2.73 (strong wind)	10
TiO_2 wedges on candle soot/PDMS	Fog	Yes	0.89	8
Micro-topographies (pillars/trapezoids/honeycombs) on PDMS	Fog	Yes	4.39	This work
Micro-topographies (pillars/trapezoids/honeycombs) on PDMS substrate with different biphilic patterns	Dew	Yes	0.0417 0.0408 0.0717	This work

1000 µm spots yielded 0.0717 *versus* 0.0230 g cm^{-2} h^{-1} for 500 µm and on pillars, 0.0650 *versus* 0.0300 g cm^{-2} h^{-1}. At 90% RH ΔT = 5 °C, the optimal size depended on the underlying micro topography: trapezoids still favored 1000 µm (0.0408 *vs*. 0.0140 g cm^{-2} h^{-1}), while in pillars, 500 µm spots performed slightly better (0.0347 *vs*. 0.0265 g cm^{-2} h^{-1}).

The surfaces presented in this work stand out as a significant advancement in atmospheric water harvesting by achieving a rare balance between high-performance metrics and environmental sustainability. While established literature often relies on specialized, non-green coatings—such as fluorinated HDFS (Gunarasan & Lee) or PFAS-based PIB rubber (Gerasopoulos *et al.*)—to achieve high collection rates, our designs utilize a PFAS-free, green chemistry approach without sacrificing efficiency. In terms of quantitative impact, the biphilic surfaces with stripes realized on pillars demonstrate a remarkable 156% gain for dew collection compared to the untreated PDMS, which is comparable with other examples in the literature in fog collection modes, our superhydrophobic pillar based surface reached a peak WCR of 4.39 g cm^{-2} h^{-1}, outperforming the high-wind results of copper-epoxy spots (2.73 g cm^{-2} h^{-1}) and bio-inspired TiO_2 wedges (0.89 g cm^{-2} h^{-1}). In Table 2 the performance of the surfaces presented here are compared to existing literature examples.

4. Conclusions

We established a scalable, PFAS-free fabrication route for biphilic surfaces for passive atmospheric water harvesting, by combining micro-textured topographies enabling the realization of highly hydrophobic and superhydrophobic surfaces, which are then patterned with stencils using PEG8000 to create biphilic surfaces. In particular, three topographies—pillars (5.5 µm), square-based trapezoids (7 µm), and honeycombs (15 µm) were paired with four biphilic geometries: 500 µm spots, 1000 µm spots, 1000 : 1000 µm stripes, and 1000 : 2000 µm stripes. All surfaces maintained extreme wettability contrast, with different wettability properties up to superhydrophobic with water contact angles above 150° and hysteresis below 10°, and areas with hydrophilic and superhydrophilic properties. This enabled a systematic exploration of how microstructure and biphilic pattern design modulate fog and dew collection.

Dew collection revealed clear, regime-specific optima shaped by the interplay of droplet mobility and nucleation sites density. Under intermediate conditions, widely spaced 1000 : 2000 µm parallel stripes on pillar topography achieved a 156% improvement over flat PDMS. The parallel hydrophilic stripes formed continuous drainage pathways, while the superhydrophobic areas sustained efficient droplet removal. Under adverse condensation conditions, the highest performance was achieved with 1000 µm hydrophilic spots, yielding a WCR of 0.0717 g cm^{-2} h^{-1} (on trapezoids) and WCR 0.065 g cm^{-2} h^{-1} (on pillars). This improvement is possible due to the increased nucleation sites density on the hydrophilic spots and the low biphilic area coverage (25%), which is not promoting early film formation or compromising the overall water mobility of the surfaces. Finally, in terms of biphilic surface area coverage, 35% coverage with parallel stripes maximized drainage under intermediate conditions (RH 70%), while 25% coverage with 1000 µm spots maximized nucleation on trapezoids and pillars under high RH (90%).

In fog collection, in which no phase change phenomenon is taking place, wettability can improve droplet impact, capture and collection. On inherently mobile textures such as pillars and trapezoids, adding hydrophilic regions typically slightly reduced performance. The introduction of hydrophilic areas increased wetted fraction, encouraged film formation, and introduced aerodynamic drag, collectively slowing droplet shedding. In all topographies, all four biphilic patterns clustered near or below the flat PDMS WCR. It is also evident, that in fog collection low biphilic surface coverage is required (<25%), since in all samples tested WCR performance was inferior compared to superhydrophobic or flat hydrophobic PDMS.

Author contributions

Konstantinos Taliantzis: experiments, data analysis, writing – original draft. Kosmas Ellinas: writing, review & editing, supervision, funding acquisition.

Conflicts of interest

The authors declare that they have no known competing financial interests or personal relationships that could have appeared to influence the work reported in this paper.

Data availability

Data and all images, graphic used are available within the article. The authors confirm that the data supporting the findings of this study are available within the article.

Supplementary information (SI) is available. See DOI: https://doi.org/10.1039/d5nr05114b.

Acknowledgements

This research work was supported “passiVe wAter harveSTing usiNg grEen SurfaceS [VASTNESS-15250]” by the Hellenic Foundation for Research and Innovation (H.F.R.I) under the “Basic Research Financing (Horizontal support for all Sciences), National Recovery and Resilience Plan Greece 2.0”.

References

1 K. F. Kaseke and L. Wang, Fog and Dew as Potable Water Resources: Maximizing Harvesting Potential and Water Quality Concerns, *GeoHealth*, 2018, **2**(10), 327–332, DOI: 10.1029/2018GH000171.

2 M. Ahmad, A. Nighojkar and A. Plappally, *A review of the methods of harvesting atmospheric moisture*, Springer, 2024. DOI: 10.1007/s11356-023-30727-x.

3 Y. Zhu, T. C. Ho, H. H. Lee, M. K. H. Leung and C. Y. Tso, Droplet jumping physics on biphilic surfaces with different nanostructures and surface orientations under various air pressure conditions, *Cell Rep. Phys. Sci.*, 2022, **3**(4), 100849, DOI: 10.1016/j.xcrp.2022.100849.

4 M. J. Hoque, *et al.*, Biphilic jumping-droplet condensation, *Cell Rep. Phys. Sci.*, 2022, **3**(4), 100823, DOI: 10.1016/j.xcrp.2022.100823.

5 A. Ghosh, S. Beaini, B. J. Zhang, R. Ganguly and C. M. Megaridis, *Enhancing Dropwise Condensation through Bioinspired Wettability Patterning*, 2014. DOI: 10.1021/la5028866.

6 K. Taliantzis and K. Ellinas, *Green hydrophobic and superhydrophobic coatings and surfaces for water related applications: A review*, Elsevier B.V., 2025. DOI: 10.1016/j.cis.2025.103566.

7 R. Ghosh and R. Ganguly, Harvesting Water from Natural and Industrial Fogs—Opportunities and Challenges, in *Energy, Environment, and Sustainability*, Springer Nature, 2018, pp. 237–266. DOI: 10.1007/978-981-10-7233-8_9.

8 H. Zhu, *et al.*, Integration of water collection and purification on cactus- and beetle-inspired eco-friendly superwettable materials, *Water Res.*, 2021, **206**, 117759, DOI: 10.1016/J.WATRES.2021.117759.

9 Z. Zhang, *et al.*, A self-sufficient system for fog-to-water conversion and nitrogen fertilizer production to enhance crop growth, *Nat. Commun.*, 2025, **16**(1), 4926, DOI: 10.1038/s41467-025-60340-0.

10 Z. Almusaied and B. Asiabanpour, A Novel Design of Hybrid Hydrophilic-Superhydrophobic Surfaces for Fog Harvesting, *Int. J. Eng. Mater. Manuf.*, 2021, **6**(3), 152–162, DOI: 10.26776/ijemm.06.03.2021.06.

11 M. Lekmuenwai, *Water harvesting performance of biphilic surfaces*, 2024.

12 M. Khamdevi, *A systematic literature review of architecture-related dew and fog harvesting*, 2023, DOI: 10.13135/2384-8677/7492.

13 W. Pei, *et al.*, Excellent fog harvesting performance of liquid-infused nano-textured 3D frame, *Chem. Eng. J.*, 2021, **409**, 128180, DOI: 10.1016/j.cej.2020.128180.

14 Y. Qiao, *et al.*, Stable dopamine-based ink for facile fabrication of robust and efficient fog-collectors, *Mater. Today Chem.*, 2024, **42**, 102345, DOI: 10.1016/j.mtchem.2024.102345.

15 D. Nioras, K. Ellinas, V. Constantoudis and E. Gogolides, How Different Are Fog Collection and Dew Water Harvesting on Surfaces with Different Wetting Behaviors?, *ACS Appl. Mater. Interfaces*, 2021, **13**(40), 48322–48332, DOI: 10.1021/acsami.1c16609.

16 M. M. Khalil, A. Kara-Ali and M. Assad, Potential of harvesting water from fog and dew water over semi-arid and arid regions in Syria, *Water Supply*, 2022, **22**(1), 874–882, DOI: 10.2166/ws.2021.229.

17 J. Knapczyk-Korczak, P. K. Szewczyk, D. P. Ura, K. Berent and U. Stachewicz, Hydrophilic nanofibers in fog collectors for increased water harvesting efficiency, *RSC Adv.*, 2020, **10**(38), 22335–22342, DOI: 10.1039/d0ra03939j.

18 J. Li, Y. Zhou, W. Wang, F. Du and L. Ren, A bio-inspired superhydrophobic surface for fog collection and directional water transport, *J. Alloys Compd.*, 2020, **819**, 152968, DOI: 10.1016/j.jallcom.2019.152968.

19 V. Tselepi, D. Nioras, E. Gogolides and K. Ellinas, A Green Plasma-Based Micro-Nanotexturing Method to Realize Stable Superhydrophobic and Superhydrophilic Thin PET Films, *Coatings*, 2025, **15**(9), 1057, DOI: 10.3390/COATINGS15091057.

20 Y. Hou, P. Shah, V. Constantoudis, E. Gogolides, M. Kappl and H. J. Butt, A super liquid-repellent hierarchical porous membrane for enhanced membrane distillation, *Nat. Commun.*, 2023, **14**(1), 1–11, DOI: 10.1038/s41467-023-42204-7.

21 S. He, Y. Fu, W. Zhang, Z. Guo and W. Liu, Slippery liquid-infused surface with micro/nano hierarchical structures: Highly efficient fog harvesting, *Friction*, 2025, 9440969, DOI: 10.26599/frict.2025.9440969.

22 X. Li, G. Wang, B. Zhan, S. Li, Z. Han and Y. Liu, A Novel Icephobic Strategy: The Fabrication of Biomimetic Coupling Micropatterns of Superwetting Surface, *Adv. Mater. Interfaces*, 2019, **6**(19), 1900864, DOI: 10.1002/admi.201900864.

23 D. Gurera and B. Bhushan, Designing bioinspired surfaces for water collection from fog, *Philos. Trans. R. Soc., A*, 2019, **377**(2138), 20180269, DOI: 10.1098/rsta.2018.0269.

24 M. Gürsoy, *et al.*, Bioinspired fog capture and channel mechanism based on the arid climate plant Salsola crassa, *Colloids Surf., A*, 2017, **529**, 195–202, DOI: 10.1016/j.colsurfa.2017.05.071.

25 G. Tian, C. Fu and Z. Guo, Biomimetic Fog Collector with Hybrid and Gradient Wettabilities, *ACS Appl. Mater. Interfaces*, 2024, **16**(33), 43694–43703, DOI: 10.1021/acsami.4c06032.

26 D. Song and B. Bhushan, Enhancement of water collection and transport in bioinspired triangular patterns from combined fog and condensation, *J. Colloid Interface Sci.*, 2019, **557**, 528–536, DOI: 10.1016/j.jcis.2019.09.068.

27 L. Zhong, H. Zhu, Y. Wu and Z. Guo, Understanding how surface chemistry and topography enhance fog harvesting based on the superwetting surface with patterned hemispherical bulges, *J. Colloid Interface Sci.*, 2018, **525**, 234–242, DOI: 10.1016/j.jcis.2018.04.061.

28 B. El Pinchasik, M. Kappl and H. J. Butt, Small Structures, Big Droplets: The Role of Nanoscience in Fog Harvesting,

ACS Nano, 2016, **10**(12), 10627–10630, DOI: 10.1021/acsnano.6b07535.

29 M. Li, S. Xie, G. Tian and Z. Guo, Biomimetic Fog Harvesting with Synergistic Effects of Multiple Driving Forces, *Langmuir*, 2025, **41**(6), 4369–4378, DOI: 10.1021/acs.langmuir.4c05155.

30 P. Sarkiris, *et al.*, Topography Optimization for Sustainable Dropwise Condensation: The Critical Role of Correlation Length, *Adv. Funct. Mater.*, 2024, **34**(1), 2306756, DOI: 10.1002/ADFM.202306756.

31 K. Gerasopoulos, W. L. Luedeman, E. Ölçeroglu, M. McCarthy and J. J. Benkoski, Effects of Engineered Wettability on the Efficiency of Dew Collection, *ACS Appl. Mater. Interfaces*, 2018, **10**(4), 4066–4076, DOI: 10.1021/ACSAMI.7B16379.

32 D. Seo, J. Lee, C. Lee and Y. Nam, The effects of surface wettability on the fog and dew moisture harvesting performance on tubular surfaces, *Sci. Rep.*, 2016, **6**, 24276, DOI: 10.1038/srep24276.

33 A. Lee, M. W. Moon, H. Lim, W. D. Kim and H. Y. Kim, Water harvest via dewing, *Langmuir*, 2012, **28**(27), 10183–10191, DOI: 10.1021/la3013987.

34 T. M. Thomas, P. Sinha Mahapatra, R. Ganguly and M. K. Tiwari, Preferred Mode of Atmospheric Water Vapor Condensation on Nanoengineered Surfaces: Dropwise or Filmwise?, *Langmuir*, 2023, **39**(15), 5396–5407, DOI: 10.1021/acs.langmuir.3c00022.

35 H. Yue, Q. Zeng, J. Huang, Z. Guo and W. Liu, *Fog collection behavior of bionic surface and large fog collector: A review*, Elsevier B.V., 2022. DOI: 10.1016/j.cis.2021.102583.

36 R. L. Farnum, Fog Harvesting, in *Unconventional Water Resources*, Springer International Publishing, 2022, pp. 51–71. DOI: 10.1007/978-3-030-90146-2_3.

37 Y. Hou, Y. Shang, M. Yu, C. Feng, H. Yu and S. Yao, Tunable Water Harvesting Surfaces Consisting of Biphilic Nanoscale Topography, *ACS Nano*, 2018, **12**(11), 11022–11030, DOI: 10.1021/acsnano.8b05163.

38 M. M. Chehrghani, T. Abbasiasl, A. K. Sadaghiani and A. Koşar, Biphilic Surfaces with Optimum Hydrophobic Islands on a Superhydrophobic Background for Dropwise Flow Condensation, *Langmuir*, 2021, **37**(46), 13567–13575, DOI: 10.1021/acs.langmuir.1c01844.

39 J. P. Chakrapani Gunarasan and J.-W. Lee, Active Surface Area-Dependent Water Harvesting of Desert Beetle-Inspired Hybrid Wetting Surfaces, *Langmuir*, 2024, **40**(10), 5499–5507, DOI: 10.1021/acs.langmuir.4c00020.

40 D. Nioras, K. Ellinas and E. Gogolides, Atmospheric Water Harvesting on Micro-nanotextured Biphilic Surfaces, *ACS Appl. Nano Mater.*, 2022, **5**(8), 11334–11341, DOI: 10.1021/ACSANM.2C02439.

41 X. Yan, *et al.*, Atmosphere-Mediated Scalable and Durable Biphilicity on Rationally Designed Structured Surfaces, *Adv. Mater. Interfaces*, 2020, **7**(13), 2000475, DOI: 10.1002/admi.202000475.

42 D. Nioras, E. Gogolides and K. Ellinas, Durable Surfaces of Both Wettability Extremes with Stable Dew Harvesting Performance During Liquid-Vapor-Phase Transitions, *Ind. Eng. Chem. Res.*, 2024, **63**(48), 20872–20882, DOI: 10.1021/ACS.IECR.4C02374.

43 H. Sun, *et al.*, *Bioinspired micro- and nanostructures used for fog harvesting*, Springer Science and Business Media Deutschland GmbH, 2021. DOI: 10.1007/s00339-021-04619-1.

44 B. Bhushan, *Design of water harvesting towers and projections for water collection from fog and condensation*, Royal Society Publishing, 2020. DOI: 10.1098/rsta.2019.0440.

45 S. Shukla, *et al.*, Nature-inspired self-similar carbon nanotubes-nonwoven nanostructured materials for fog harvesting applications, *Compos. Commun.*, 2023, **43**, 101694, DOI: 10.1016/j.coco.2023.101694.

46 E. Philander and T. Saito, Fog harvesting behavior on alternating vertical hydrophobic-hydrophilic stripes, *Results Eng.*, 2025, **26**, 105056, DOI: 10.1016/j.rineng.2025.105056.

47 Y. Fu, L. Wu, S. Ai, Z. Guo and W. Liu, Bionic collection system for fog-dew harvesting inspired from desert beetle, *Nano Today*, 2023, **52**, 101979, DOI: 10.1016/j.nantod.2023.101979.

48 M. Zarei, B. Dabir, N. Esmaeilian and D. M. Warsinger, Biomimetic bumpy and eco-friendly slippery surfaces for enhanced dew and fog water harvesting, *J. Water Process Eng.*, 2025, **70**, 106950, DOI: 10.1016/j.jwpe.2025.106950.

49 S. Lee and J. Lee, Improvement of humid air condensate drainage through bi-philic patterned surfaces, *Int. J. Heat Mass Transfer*, 2022, **194**, 123097, DOI: 10.1016/j.ijheatmasstransfer.2022.123097.

50 M. M. Garimella, S. Koppu, S. S. Kadlaskar, V. Pillutla, Abhijeet and W. Choi, Difference in growth and coalescing patterns of droplets on bi-philic surfaces with varying spatial distribution, *J. Colloid Interface Sci.*, 2017, **505**, 1065–1073, DOI: 10.1016/j.jcis.2017.06.099.

51 Y. Fu, S. Ai, Z. Guo and W. Liu, Biomimetic 3D efficient fog harvester by synergistic wettability effect, *J. Colloid Interface Sci.*, 2023, **649**, 646–654, DOI: 10.1016/j.jcis.2023.06.142.

52 J. Estephan, *et al.*, Controlled wettability of biphilic patterned surfaces for enhanced atmospheric water harvesting, *Micro Nano Eng.*, 2024, **23**, 100255, DOI: 10.1016/J.MNE.2024.100255.

53 J. B. Boreyko, R. R. Hansen, K. R. Murphy, S. Nath, S. T. Retterer and C. P. Collier, Controlling condensation and frost growth with chemical micropatterns, *Sci. Rep.*, 2016, **6**(1), 19131, DOI: 10.1038/srep19131.

54 J. Zhang, C. Yang, Z. Qu, Z. Li and X. Li, Dynamics of Condensing Droplets Driven by Multidirectional Laplace Pressure Gradients on Hierarchical Microstructured Surfaces, *ACS Appl. Mater. Interfaces*, 2025, **17**(34), 48989–48999, DOI: 10.1021/acsami.5c10919.

55 D. Beysens, Dew nucleation and growth, *C. R. Phys.*, 2006, **7**(9–10), 1082–1100, DOI: 10.1016/J.CRHY.2006.10.020.